Available online at www.sciencedirect.com
SCIENCE DIRECT
Journal of Magnetic Resonance 181 (2006) 98–106
JMR Journal of Magnetic Resonance
www.elsevier.com/locate/jmr

Rapid MRI method for mapping the longitudinal relaxation time

Jung-Jiin Hsu *,[1], Gary H. Glover

Richard M. Lucas Center for Imaging, Stanford University, 1201 Welch Road MC 5488, Stanford, CA 94305-5488, USA

Received 17 December 2005; revised 19 March 2006
Available online 18 April 2006

Abstract

A novel method for mapping the longitudinal relaxation time in a clinically acceptable time is developed based on a recent proposal [J.-J. Hsu, I.J. Lowe, Spin–lattice relaxation and a fast T_1-map acquisition method in MRI with transient-state magnetization, J. Magn. Reson. 169 (2004) 270–278] and the speed of the spiral pulse sequence. The method acquires multiple curve-fitting samples with one RF pulse train. It does not require RF pulses of specific flip angles (e.g., 90° or 180°), nor are the long recovery waiting time and the measurement of the magnetization at thermal equilibrium needed. Given the value of the flip angle, the curve fitting is semi-logarithmic and not computationally intensive. On a heterogeneous phantom, the average percentage difference between measurements of the present method and those of an inversion–recovery method is below 2.7%. In mapping the human brain, the present method, for example, can obtain four curve-fitting samples for five 128×128 slices in less than 3.2 s and the results are in agreement with other studies in the literature.

Keywords: Spin–lattice relaxation; Longitudinal relaxation; T_1 map; Fast imaging; Spiral pulse sequence

1. Introduction

Mapping the longitudinal (spin–lattice) relaxation time T_1 usually involves obtaining samples for curve-fitting the time constant of the relaxation equation

$$M_z(t) = M_0 e^{-t/T_1} + M_{eq}(1 - e^{-t/T_1}), \quad (1)$$

where M_z is the longitudinal magnetization as a function of time t, M_0 the initial magnetization at $t = 0$, and M_{eq} the thermal-equilibrium (i.e., fully relaxed) magnetization. Conventionally, this curve is sampled by repeated use of the 180°-τ-90° (inversion–recovery, IR) [1] or the 90°-τ-90° (saturation–recovery, SR) [2] pulse sequences with various sample times τ. These methods are time consuming mainly because each repetition obtains only one sample.

T_1 mapping as a quantitative approach in medicine is hampered by its lengthy scan time. In a recent paper [3], a fast mapping method is introduced which does not have the drawbacks of the IR and SR methods and promises reduced scan time in clinical applications. A main feature is time-saving by acquiring multiple curve-fitting samples with one RF pulse train, which is similar to the data acquisition by the Carr–Purcell pulse train [4] for curve-fitting the transverse relaxation time. In addition, measurement of M_{eq} and long delays for full recovery of the magnetization are not necessary. The curve to fit is a decay exponential function instead of the recovery exponential one of Eq. (1). It is shown [3] that the results obtained from the new method are in agreement with that of the IR method.

This article reports the development of this fast method for T_1 mapping in a clinical setting and the results of application to the human brain. In the original paper [3], the image reciprocal domain (the k-space) is sampled by a low-flip-angle multiple-shot method—the rotating ultra fast imaging sequence, RUFIS [3,5–8]. In this work, the k-space is sampled by a single-shot pulse sequence to utilize

* Corresponding author. Fax: +1 650 723 5795.
E-mail address: jjhsu@stanford.edu (J.-J. Hsu).
[1] Also known as Jason Hsu.

1090-7807/$ - see front matter © 2006 Elsevier Inc. All rights reserved.
doi:10.1016/j.jmr.2006.03.014

a larger flip angle for better signal-to-noise ratio; a spiral pulse sequence [9] is employed for this purpose and for its speedy k-space sampling capability. In addition, multi-slice acquisition is implemented. In mapping the human brain, the present method, for example, can obtain four curve-fitting samples for mapping five 128×128 slices in less than 3.2 s and the T_1 values are in agreement with other studies in the literature. The new features of the present method in comparison with other popular methods such as IR, SR, and Look–Locker's [10] are elaborated in Section 4.

2. Method

2.1. Theory

Consider the NMR pulse sequence shown in Fig. 1. The pulse sequence is composed of a curve-sampling RF pulse train of common flip angle α, a recovery delay D_R, a 180° inversion RF pulse, and a post-inversion delay D_P. The first and the second halves of the sampling pulse train (as divided at the 180° inversion RF pulse) have an identical set of inter-pulse spacings τ_i. Suppose that the transverse magnetization $M_\perp$ when each α RF pulse is applied has irreversibly relaxed, i.e., $M_\perp = 0$, so no transverse magnetization is transformed to the longitudinal direction by the α RF pulse. This condition is satisfied if the RF pulse spacing is much longer than the transverse relaxation time T_2, or is approximately satisfied for dephased $M_\perp$ (which also results in $M_\perp = 0$) if α is small. Assume that the length of the RF pulses is negligible. In the first half of the pulse train, the NMR signal following the i-th RF pulse is proportional to the volume integral of the transverse magnetization $M_{\perp(i)}$

$$M_{\perp(i)} = (M_0 \cos^{i-1}\alpha\, e^{-t_i/T_1} + C_i)\sin\alpha, \tag{2}$$

where M_0 is the initial longitudinal magnetization at time $t = 0$, t_i is the time when the i-th RF pulse is applied, and

$$C_1 = M_{eq}(1 - e^{-t_1/T_1}), \tag{3}$$

$$C_i = C_{(i-1)}e^{-\tau_{(i-1)}/T_1}\cos\alpha + M_{eq}(1 - e^{-\tau_{(i-1)}/T_1}), \quad i > 1 \tag{4}$$

{see Eqs. (7), (8), (12), and (13) of [3] with $N = 1$, $n = 1$, $\Delta = 0$, and $D_i = \tau_{(i-1)}$}. The expression for C_i's is a function of T_1, M_{eq}, α, and τ_i but is not a function of M_0. In the parentheses of Eq. (2), the first term is referred to as the *decay* or M_0 *term* and the second term the *recovery term*. The second half of the pulse train has the same expressions but the sign of the M_0 term is reversed because of the inversion RF pulse; yet the recovery term remains the same. Subtraction of the data from the two half-trains therefore eliminates the recovery term, which also eliminates the need for measuring M_{eq}. The subtraction of the two data sets followed by division by $\cos^{i-1}\alpha$ results in

$$\bar{M}_{\perp(i)} = \lambda(1 + \beta)M_0 e^{-t_i/T_1}\sin\alpha, \tag{5}$$

where β is a constant representing the effects of magnetization recovery during D_R and D_P, and the error of the flip angle of the inversion RF pulse. The division is termed *normalization*. In Eq. (5), λ is a constant representing the effect of magnetization saturation when the pulse sequence in Fig. 1 is repeated and the signals are summed. The value of λ depends on the degree of magnetization recovery before each repetition. For example, if each of N repetitions starts with the identical value of M_0, then λ will be N. For single execution of the pulse sequence, $\lambda = 1$. Eliminating the need of measuring M_{eq} is a feature shared by the CREPE method of Zhao et al. [11], in which M_{eq} appears only in the intercept of a linear equation and T_1 can be determined solely by the equation's slope.

Eq. (5) is an exponential decay with a time constant $1/T_1$. The value of T_1 can be obtained through curve fitting the normalized signals. If the magnetization is spatially encoded for MRI, the same principle applies to the normalized images reconstructed from the post-subtraction signals. Because T_1 is the quantity sought, β need not be unity, nor are the actual values of λ, M_0, and $\sin\alpha$ relevant in determining T_1. Consequently, imperfect flip angle of the inversion RF pulse is tolerable and full magnetization recovery before the inversion and before each repetition is not necessary.

2.2. Pulse sequence and image processing

Following Hsu and Lowe [3], a T_1 map is constructed as follows:

1. The NMR pulse sequence shown in Fig. 1 is executed (referred to as one scan). The longitudinal magnetization at time $t = 0$, i.e., M_0, can be arbitrary. It is not neces-

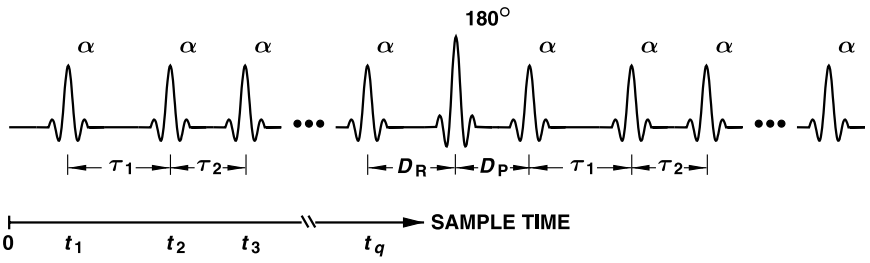

Fig. 1. Pulse sequence for acquiring q samples for curve-fitting the longitudinal relaxation time (only the RF amplitude modulation is shown). Acquisition of imaging data follows each α RF pulse; in this work, a two-dimensional spiral scan is employed.

sary for the RF pulses in the train to be equally spaced but the spacing should allow the transverse magnetization to relax to zero. Similarly, the post-inversion delay is not mandatory if the inversion produces no or negligible transverse component. If $\tau_i \ll T_1$, multiple RF pulses can be included in the train.

2. Each of the signals from the second half of the pulse train is subtracted from the corresponding signal from the first half and an image is reconstructed from the post-subtraction signal. The raw images are then normalized by division with $\cos^{i-1}\alpha$.
3. The normalized images are the samples of the exponential decay curve at time t_i and are curve-fitted, pixel by pixel, to obtain the decay time constant, which is equal to $1/T_1$.

2.3. Curve fitting for T_1

Linearized least χ^2 fitting is used in this work with χ^2 defined by (see, for example, [12])

$$\chi^2 = \sum_i \frac{|y_i - \ln a - bt_i|^2}{\sigma_i^2} \tag{6}$$

and $y_i = \ln(p_i/\cos^{i-1}\alpha)$, where p_i is the pixel value of the raw image of time t_i and $b = -1/T_1$ (i.e., fitting with semi-log coordinates). The intercept $\ln a$ is irrelevant in constructing the T_1 map. The uncertainty σ_i is given by (see, for example, [12])

$$\sigma_i = \frac{dy_i}{dp_i}\sigma = \frac{1}{p_i}\sigma, \tag{7}$$

where the differentiation accounts for the transformation from Cartesian to logarithmic coordinates and σ is the uncertainty of the raw pixel value p_i. In this work, σ is assumed to have a common value among all raw images and is set to unity. In Eq. (6), the quantity $1/\sigma_i^2$ can be thought of as the weight of the i-th curve sample. Note that although the normalized pixel values $p_i' = p_i/\cos^{i-1}\alpha$ are used in the curve fitting, the weight is p_i^2/σ^2 from Eq. (7), not $p_i'^2/\sigma^2$.

2.4. Experimental

The condition of $T_2 \ll \tau_i < T_1$ ideal for the present method is satisfied in the human brain. For example, at 1.5 T, T_2 of the white matter (WM) is ~75 ms, the gray matter (GM) ~90 ms [13–16], and T_1 longer than 500 ms. The shortest RF pulse spacing in this work is 300 ms. Thus the transverse magnetization can relax between the α RF pulses and multiple α RF pulses can be applied in a period of a few T_1's. The cerebrospinal fluid (CSF) has very long T_2 (~2600 ms [15]); its result may not be as accurate under the current pulse sequence parameters.

Multiple slices can be acquired within the time for one scan. Pulse sequences of Fig. 1, each sampling a difference slice, can be superimposed such that the time between the data acquisitions of one slice is interleaved with data acquisitions of other slices. The number of slices that can be acquired is therefore determined by the pulse spacing minimum.

The value of flip angle α is needed for constructing the T_1 maps since it is not treated as a curve-fitting parameter in this work. Given the length of an RF pulse, modern MRI scanners can automatically determine the output power to meet the angle specified by the scanner operator with fair accuracy and precision, for example, $\pm 1.2°$ standard deviation across the volume of interest with the RF coils used in this work. Nevertheless for an accurate assessment of the present method, the actual flip angle is obtained from a map constructed by solving a trigonometry relation between the pixel intensity of the images obtained from a α RF pulse and a 2α RF pulse. For the inversion RF pulse, the actual flip angle is not measured.

The experiments were carried out at 1.5 T with a commercial clinical MRI scanner (Signa Excite, GE Medical Systems, Milwaukee, WI). The spiral scan acquired k-space data from the origin outwards in size equivalent to a Fourier-transformation matrix of 128×128 and $T_E = 7$ ms. The setting of sample times was meant to demonstrate multislice acquisition and that the RF pulse train can be unequally spaced; the setting was not necessarily optimal. For multiscan experiments, the signals were averaged prior to the curve fitting. Since only the relative time among samples is relevant in the curve fitting, the sample times for the present method were quoted such that the first sample time was 0 ms. In the curve fitting, the decay was assumed to be mono-exponential. All RF pulses in Fig. 1 were slice-selective and the length of the RF pulses was 6.4 ms, which was assumed to be negligible. The experiments involving human subjects were approved by the University's institutional review board.

A phantom was constructed for comparison between the present method and an IR method. The phantom contained four agar-gel specimens of various T_1 values. The specimens were prepared by thermally dissolving 1.5% (by weight) dry agar in saline doped with Gd-DTPA of different concentrations. Each specimen was dispensed into two plastic, cylindrical vials of 3.4-cm diameter and 8.7-cm height and allowed to solidify. Seven of the vials were bundled and centered in a plastic, cylindrical jar of 14.2-cm diameter and 25-cm height. The jar was topped up with Gd-DTPA doped saline to homogenize the external magnetic field. When the phantom was positioned in the magnet of the scanner, all axes of the cylinders were parallel to the direction of the external magnetic field. The MRI slice selection was transverse (Fig. 2). The arrangement of the vials was meant to avoid matching the symmetry of the receiver coil and the symmetry formed by the locations of the same specimens. The pulse program for the IR method was a product of the scanner manufacturer; it implemented the pulse sequence of 180°-τ-90°-T_E/2-180°-T_E/2-ACQ [17]. Each data acquisition (ACQ) read one line

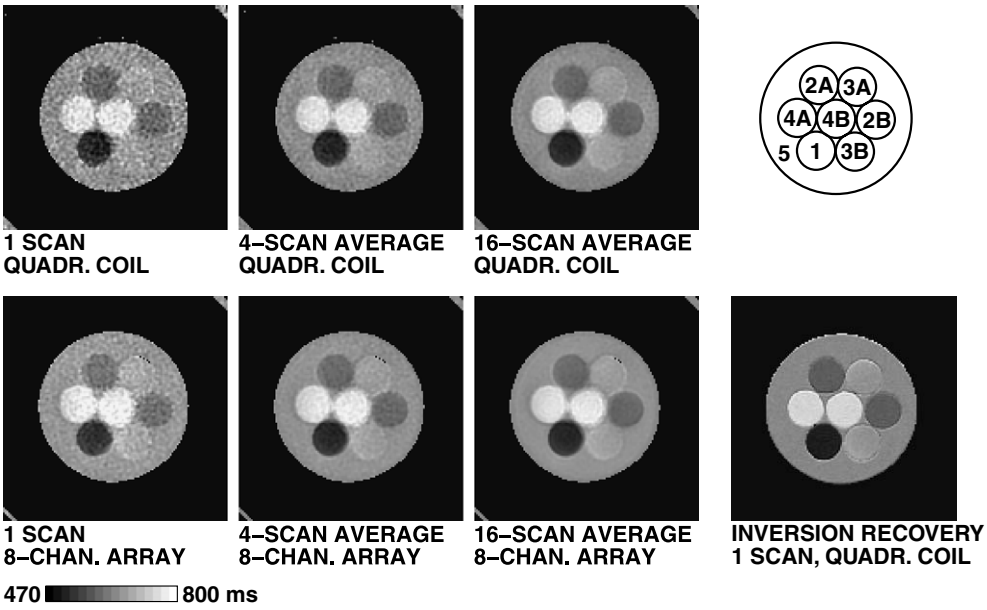

Fig. 2. T_1 maps of the phantom and vial reference labels. Maps in the left three columns are obtained by the present method [3].

of the discrete Cartesian k-space of size 128×128 (i.e., spin-warp imaging). The T_1 values were obtained by a three-parameter fitting of Eq. (1). The IR pulse program had a constraint of $\tau \leqslant 4$ s, which set the upper limit of the T_1 value in preparing the specimens because a curve-fitting sample at $\tau = 5T_1$ was desired. With a sample at such long τ value, the relaxation curve would be represented properly and thus, under the influence of the noise, the T_1 results were expected to be less dependent on the fitting method chosen.

3. Results

3.1. Benchmarking

The T_1 maps of the phantom are shown in Fig. 2. Vials with content dispensed from the same specimen are labeled with the same arabic numeral. Referred to Fig. 1, $q = 4$, $\alpha = 30°$, $D_R = 1000$ ms, $D_P = 10$ ms, $T_E = 5$ ms, and sample-time set $t_i \in \{0, 625, 1000, 1375\}$ ms. For multiscan experiments, the interscan delay was 2 s. For the IR method, $T_E = 9$ ms, the sample-time set was $\tau_i \in \{70, 625, 1000, 1375, 4000\}$ ms, and a 6-s delay for full magnetization recovery was executed before scanning the next k-space line. The slice thickness was 5 mm and the field-of-view 22 cm.

In Fig. 2, the precision of the maps is improved by enhancing the signal-to-noise ratio through multiscan averaging. Using a multichannel receiver coil also delivers the same effect. The high signal-to-noise ratio of the IR T_1 map is attributed to the use of fully recovered magnetization and large flip angle, i.e., 90° versus $\alpha = 30°$.

The T_1 values are collected in Table 1; they are the averages and the standard deviations of 5×5 pixels at the centers of each vial. Note that the T_1 values in vials containing

Table 1
T_1 values of the phantom (in ms)

	Vial							5
	1	2A	2B	3A	3B	4A	4B	
Method of Hsu and Lowe [3] with spiral scan								
1 scan, QC	499 (23)	598 (19)	599 (20)	673 (24)	679 (23)	790 (29)	783 (33)	660 (25)
4-scan average, QC	502 (8)	598 (8)	596 (13)	678 (12)	675 (11)	780 (13)	779 (15)	655 (11)
16-scan average, QC	501 (5)	599 (5)	599 (7)	676 (6)	678 (4)	773 (12)	783 (10)	652 (6)
1 scan, 8CH	523 (11)	624 (9)	608 (17)	702 (16)	696 (13)	774 (18)	804 (26)	660 (10)
16-scan average, 8CH	508 (4)	602 (5)	599 (4)	680 (6)	677 (5)	768 (4)	781 (5)	659 (2)
Inversion–recovery with spin-warp scan								
1 scan, QC	493 (5)	586 (4)	584 (3)	660 (7)	664 (5)	754 (5)	754 (5)	644 (4)
T_2	82 (1)	83 (1)	84 (1)	84 (1)	84 (1)	88 (1)	88 (1)	373 (11)

A quadrature head coil (QC) and an eight-channel array head coil (8CH) are employed for signal reception. The numbers in the parentheses are the standard deviations of the 25 pixels in the region of interest.

the same specimen are reproduced. The agreement with the IR results suggests that the present method is capable of accurately obtaining T_1 values in very short scan time. All experiments were performed in a continuous block of time to minimize the probability of scan environment change and scanner performance variation. The scan time was 3.8 s for 1-scan and 1 min and 30 s for 16-scan experiments for the present method.

The apparent transverse relaxation times T_2 are also tabulated, which are estimated by two spin-echo scans of echo time $T_E = 10$ and 100 ms, respectively; the short T_2 of the specimens confirms that the condition $T_2 \ll \tau_i$ was satisfied.

3.2. T_1 map of the brain

The anatomic image and T_1 maps of the brain of a normal participant (Subject I) are shown in Fig. 3. The anatomic image was acquired by fast spin-echoes ($T_E = 68$ ms and $T_R = 3000$ ms). The T_1 maps were acquired with, referred to Fig. 1, $q = 4$, $\alpha = 30°$, $D_R = 1000$ ms, $D_P = 10$ ms, $T_E = 5$ ms, and sample-time set $t_i \in \{0, 500, 800, 1100\}$ ms. For multiscan experiments, the interscan delay was 2 s. The slice thickness was 5 mm, space between slices 2 mm, and the field-of-view 22 cm. All scans were performed with a quadrature RF head coil.

In Fig. 3, the time to obtain the data for all the five slices in the 1-scan experiment was 3.2 s. Although noisy, the 1-scan map properly captures the anatomic structure of the brain in comparison with the anatomic image. The noise situation is reduced by multiscan averaging. The improvement becomes marginal beyond 4 scans; both 4-scan and 32-scan experiments generate T_1 maps of very good quality. The 4-scan experiment took 18.8 s to complete and the 32-scan one took 2 min and 44 s.

The average T_1 values and the standard deviations in some regions of interest are collected in Table 2. Each region contains nine contiguous pixels, equivalent to a volume of 0.133 cm^3. The table includes results of various

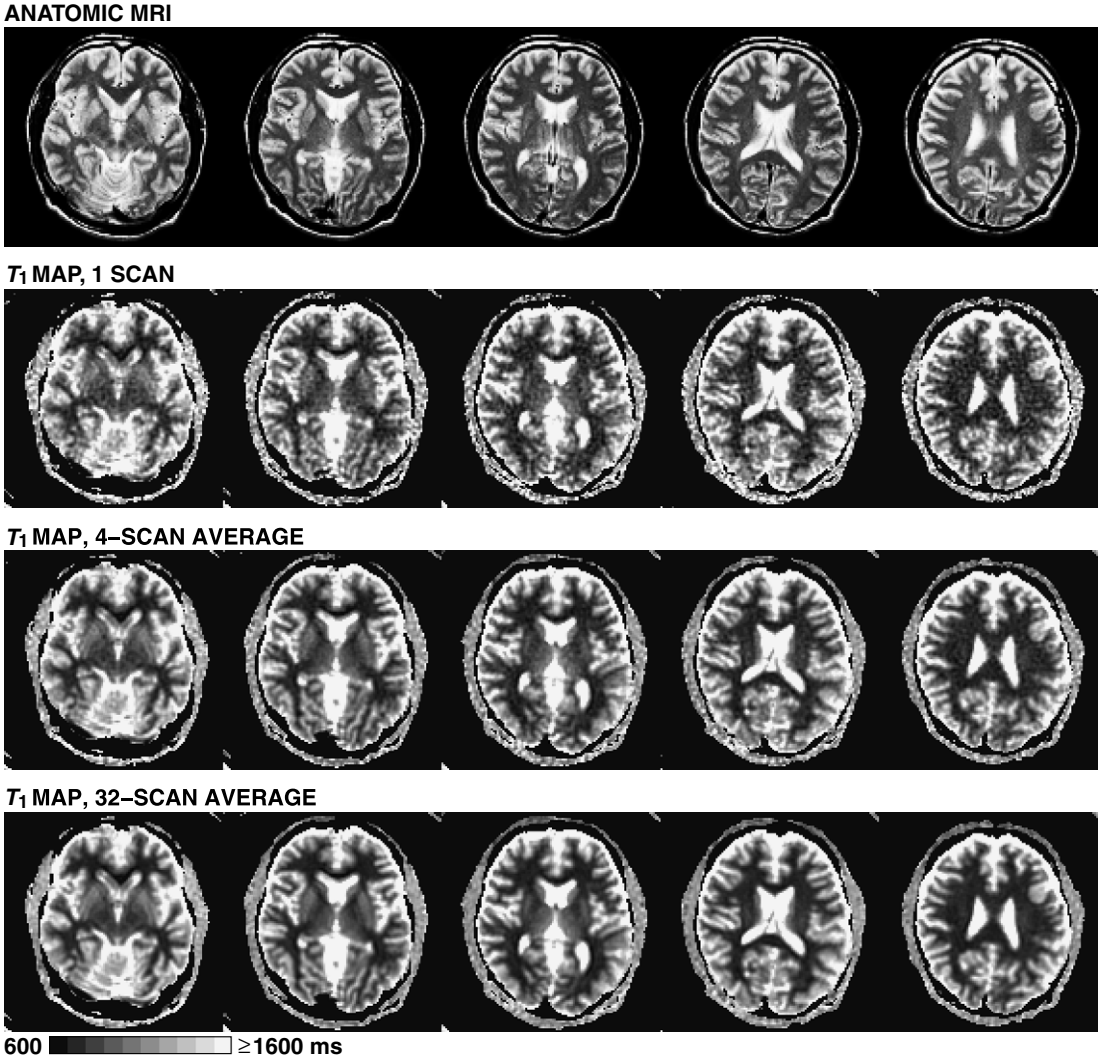

Fig. 3. Anatomic image and T_1 maps of the brain constructed from various data sets as indicated. The contrast and brightness of the anatomic image is adjusted for comparison with the T_1 maps. The gray scale represents the T_1 value in the T_1 maps.

Table 2
T_1 values of the human brain at 1.5 T (in ms)

	Frontal WM	Splenium[a]	Occipital WM	Thalamus	Putamen	Caudate[b]
This work, Subject I (male, age 39)						
1 scan	727 (62)	680 (53)	698 (52)	890 (22)	1044 (54)	1079 (54)
4-scan average	697 (19)	685 (23)	661 (23)	879 (31)	1033 (37)	1064 (27)
32-scan average	677 (11)	677 (14)	675 (9)	869 (20)	999 (14)	1050 (26)
This work, Subject II (female, age 31)						
1 scan	689 (28)	683 (55)	700 (53)	920 (65)	1012 (53)	1082 (59)
4-scan average	684 (19)	710 (39)	705 (27)	903 (37)	1014 (20)	1088 (41)
32-scan average	669 (10)	687 (13)	711 (14)	891 (24)	1019 (22)	1071 (24)
This work, five subjects						
Average	655	683	680	885	994	1059
[min., max.]	[629, 677]	[659, 719]	[632, 747]	[868, 915]	[949, 1019]	[1031, 1085]
Cho et al. [35], $n = 115$	641 (27)	635 (40)	656 (22)	857 (47)	928 (68)	1052 (59)
van Walderveen et al. [29], $n = 10$	701 (45)	706 (53)	720 (31)	907 (71)	1024 (64)	1140 (93)

For this work, the numbers in the parentheses are the standard deviations of the nine pixels in the region of interest, while for other references, are the standard deviations among n subjects.
[a] Splenium of corpus callosum.
[b] Head of caudate nucleus.

degree of scan averaging for two participants. The reduction of the standard deviations concurs with the improvement in signal-to-noise ratio by multiscan averaging. The table also lists the statistics based on the 32-scan experiments of Subjects I and II together with 8-scan experiments of three additional participants (female, age 26; male, age 27; female, age 35). All T_1 values are in agreement with results from other statistical studies on a larger number of subjects, which are also tabulated in Table 2. The agreement suggests that the present method with spiral scan is effective in obtaining accurate T_1 maps of the brain.

4. Discussion

4.1. Time saving

In IR and SR methods, the total scan time is determined by the sum of all the sample times t_i and recovery delays D'_R. Thus, for q samples, the total scan time is $\sum_{i=1}^{q} t_i + qD'_R$ and an additional sample with extended sample time may be needed to represent M_{eq}. Variants of the IR method reduce the scan time by eliminating the need for full recovery and M_{eq} (see, for example, [18,19] and references therein). For example, the MFIR method of Gupta et al. [18] can collect all the samples in time $q\Delta$, where $t_q \leqslant \Delta < D'_R$. In the present method, a sample at extended time is not necessary and because the samples are acquired in one scan, the total scan time is mainly determined by the longest sample time, i.e., $2t_q + 2D_R$, where $D_R \ll D'_R$ (because full recovery of the magnetization is not required), which can reduce the scan time considerably in particular for scanning tissues with long T_1.

4.2. Look–Locker's method

The method of Look and Locker [10] is also a pulse-train method in which a sequence of equally spaced RF pulses is applied until the magnetization reaches a steady state (SS). If $M_{\perp(SS)}$ and the relation between $M_{\perp(1)}$ and M_{eq} are known, T_1 can be solved from a equation involving the slope of the line fitted on a plot of $\ln(M_{\perp(i)} - M_{\perp(SS)})$ versus i. By contrast the present method need not establish a steady state and the RF pulses need not be equally spaced. In fact, because the magnetization is in a transient state during the Look–Locker's pulse train, the present method [3] can be utilized to determine the value of T_1 by regrouping the acquired signals, as discussed in Section 4.5 below.

4.3. Flip-angle dependence

In the present method, the flip angle α is not required to be at specific values. The value of α is used in performing the $\cos^{i-1}\alpha$ division. If the value of α were off by, for example, +3°, the T_1 values of Subject I for the frontal WM, thalamus, and putamen would have been 5.8%, 8.1%, and 9.3% higher, respectively. Derived in Appendix A, the fractional error of the relaxation time $\Delta T_1/T_1$ is approximately given by

$$\frac{\Delta T_1}{T_1} = \frac{T_1}{\tau} \tan\alpha \, \Delta\alpha, \tag{8}$$

where the RF pulse train is assumed to be equally spaced by τ. The dependence on T_1/τ and on $\tan\alpha$ is similar to that in the Look–Locker's method derived by Kay and Henkelman [20]. Thus, if the actual flip angle is uncertain (including when α is treated as a parameter in the curve fitting) and accurate results are desired, larger pulse spacing and smaller α can reduce the probability of error.

4.4. Sampling for curve fitting

Adding α RF pulses to obtain more curve-fitting samples might not be preferable because the application of α

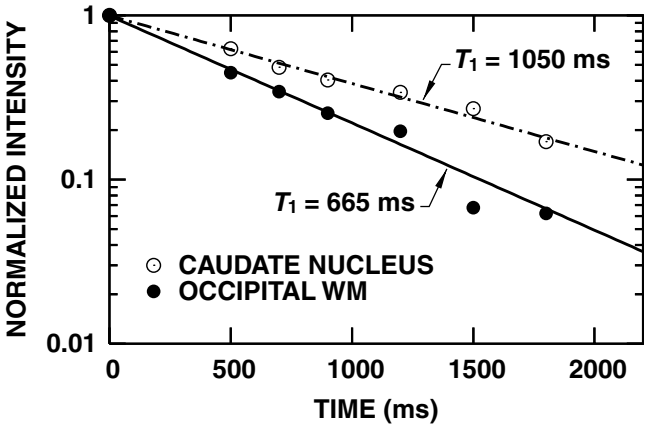

Fig. 4. Examples of the combined sample set and the curves fitted thereto. The two separate sample-time sets are $\{0, 500, 900, 1500\}$ and $\{0, 700, 1200, 1800\}$ ms, each 4-scan averaged. The legend indicates the tissues from which the two example pixels are taken.

RF pulses saps the M_0 term [cf. Eq. (2)]. Alternatively, increasing the number of curve samples can be accomplished by separate experiments of different sample-time sets. The overall coefficient of the decay exponential function of Eq. (5) may be different from experiment to experiment because of the difference in the values of M_0, λ, and β. Nevertheless a combined sample set can be formed by scaling, for each experiment, all the samples by a common factor such that the values of the first sample of all the experiments are equal. Examples are shown in Fig. 4, in which a combined set of seven samples are collected from two experiments of four samples.

Consider a material whose magnetization contains independent components of different T_1 values. Suppose that the components are A and B. Eq. (1) is rewritten as

$$M_z(t) = M_{0A}e^{-t/T_{1A}} + M_{eqA}(1 - e^{-t/T_{1A}}) + M_{0B}e^{-t/T_{1B}} + M_{eqB}(1 - e^{-t/T_{1B}}). \quad (9)$$

Following the derivation in Section 2.1, the normalized magnetization of Eq. (5) becomes

$$\bar{M}_{\perp(i)} = [\lambda_A(1+\beta_A)M_{0A}e^{-t_i/T_{1A}} + \lambda_B(1+\beta_B)M_{0B}e^{-t_i/T_{1B}}]\sin\alpha. \quad (10)$$

Thus the samples are to be fitted to a bi-exponential decay curve. To combine samples from experiments of different sample-time sets as described above, the ratio between the overall coefficients of the two exponential functions, i.e., $[\lambda_A(1+\beta_A)M_{0A}]/[\lambda_B(1+\beta_B)M_{0B}]$, must be the same in each experiment. This condition involves the selection of the sample times, the delay between pulse trains, and D_R. A simple way is to let both components of the magnetization fully recover during D_R and the inter-train delay.

4.5. Remarks

In Table 1, it is interesting that the liquid in the phantom (numbered 5 in Fig. 2 and Table 1), which fills up the voids in the jar, has $T_2 = 373$ ms, comparable to the minimum spacing of the sample times 375 ms; thus the condition $T_2 \ll \tau_i$ was not fulfilled. Nevertheless the present method still generates a T_1 value in agreement with the IR method. Recall that the condition is to ensure that the residual transverse magnetization has fully relaxed or is negligible when each α RF pulse is applied. Because the IR method is not subject to this condition, the agreement implies that the condition might not be a strict one experimentally.

In the curve fitting, the noise influences the data points unevenly because of the cosine normalization [cf. Eq. (5)]. The T_1 values are fitted from the modulus images. If the noise has zero mean (e.g., Gaussian distributed), the noise transformed to the modulus images does not necessarily have zero mean (e.g., Rician distributed). After dividing by $\cos^{i-1}\alpha$, the moduli obtained from later α RF pulses in the pulse train can be higher than the correct values. The resultant T_1 values are larger. This artifact from the normalization might have contributed to the slight deviation (below 2.7% on average) between the results from the present method and the IR method (cf. results from one-scan with a quadrature coil, Table 1).

The principle of Hsu and Lowe [3] can be understood as follows. Observe from Eqs. (1) and (2), the longitudinal relaxation can be thought of as a combination of two independent components: (i) the decay term, i.e., the decay of the initial magnetization and (ii) the recovery term, i.e., the magnetization recovery from null towards the thermal equilibrium or to the steady state. Any two identical pulse trains produce the identical recovery terms regardless of their initial magnetization. For example, consider regrouping a single pulse train of $N+1$ equally spaced RF pulses to form two pulse-trains. The train consisting of the first to the N-th pulses and the train consisting of the second to the $(N+1)$-th pulses will have the same sequence of N recovery terms; thus the subtraction of the two trains' signals eliminates the recovery terms and if the magnetization is in a transient state, i.e., the M_0 term is not zero (for example, as in the Look–Locker's pulse train), the N post-subtraction signals will satisfy Eq. (5). The regrouping mode needs only the second half of the pulse train in Fig. 1 and thus the scan time is halved. The present work utilizing the pulse sequence in Fig. 1 is merely one implementation of the principle [3] that allows unequally spaced RF pulse trains and has a larger value of the M_0 term.

Mapping T_1 in a dynamic course can be achieved with repetition of the pulse sequence in Fig. 1. T_1 maps can also be constructed from the second half of a pulse train and the first half of the next pulse train, which equivalently doubles the mapping rate. This scheme of time-series mapping is capable of obtaining T_1 values at a time resolution of, for example, 1.8 s per reading per eight slices, feasible for brain functional MRI [21]. Such speed would also meet the requirement of 2–4 s per measurement of T_1 in vivo suggested by Diesbourg et al. [22] for studies monitoring bolus

injection of contrast agent. The Look–Locker EPI method [23] and the T_1-FARM method [24] have been optimized towards dynamic mapping. Their mapping rate and accuracy are comparable to those achieved by the present work although their performance of multislice data acquisition was not demonstrated.

5. Conclusion

A novel method for rapidly mapping the longitudinal relaxation time in a clinically acceptable time is developed based on a recent method [3] and the speed of the spiral pulse sequence [9]. A main feature is the time saving by acquiring multiple curve-fitting samples with one RF pulse train. The method does not require the RF pulses be at specific values and long delays for full recovery of the magnetization are not necessary. The curve fitting is not computationally intensive. Unlike in other pulse-train methods, e.g., [10,25–28], magnetization preparation and establishing a steady state are not required. Even when with lower signal-to-noise ratio, the method can successfully obtain a proper T_1 map of the human brain with one scan in a very short period of time. Studies beginning with scout scans for quick T_1 estimates can take full advantage of the one-scan speed of the present method and quality T_1 maps can be obtained by averaging over only a few more scans.

The diagnostic value of tissue's longitudinal relaxation time is being actively explored (for example, [29–34]). The authors hope the present rapid method can be of help in facilitating dynamic studies and clinical assessment of disease.

Acknowledgments

This work is supported by NIH Grant RR09784 and the Richard M. Lucas Foundation. Acknowledgement is made to Dr. J.-Y. Cliff Hsu of UCSF for consultation and to Dr. Arundhuti Ganguly, Yanle Hu, Christine Law, Dr. Laura Pisani, Rebecca Rakow-Penner, and Dr. Yi-Shan Yang for assistance.

Appendix A

In this appendix, the error in T_1 resulted from mis-specified value of the flip angle α is estimated. Recall Eqs. (2)–(5); the curve to fit, including the α dependence explicitly, can be expressed in a simplified form

$$R_i = \cos^{i-1}\alpha\, e^{-t_i/T_1},$$

where R_i represents the data point at sample time t_i and is assumed to fit exactly on the curve. Suppose the flip angle is mis-specified by a small amount $\Delta\alpha$ and the data can still fit the form well but result in relaxation time $T_1 + \Delta T_1$, i.e.,

$$R_i = \cos^{i-1}(\alpha + \Delta\alpha)e^{-t_i/(T_1+\Delta T_1)}.$$

By the Taylor series expansion and neglecting terms higher than the second order, the above equation becomes

$$R_i = \cos^{i-1}\alpha\, e^{-t_i/T_1} + \left[\frac{t_i \Delta T_1}{T_1^2} - (i-1)\tan\alpha\,\Delta\alpha\right]\cos^{i-1}\alpha\, e^{-t_i/T_1}.$$

The first term on the right-hand side is simply R_i; thus for every R_i,

$$\frac{\Delta T_1}{T_1} = (i-1)\frac{T_1}{t_i}\tan\alpha\Delta\alpha.$$

For simplicity, assume the RF pulse train is equally spaced by τ, i.e., $t_i = (i-1)\tau$. The fractional error is then

$$\frac{\Delta T_1}{T_1} = \frac{T_1}{\tau}\tan\alpha\Delta\alpha.$$

References

[1] R.L. Vold, J.S. Waugh, M.P. Klein, D.E. Phelps, Measurement of spin relaxation in complex systems, J. Chem. Phys. 48 (1968) 3831–3832.
[2] G.G. McDonald, J.S. Leigh Jr., A new method for measuring longitudinal relaxation times, J. Magn. Reson. 9 (1973) 358–362.
[3] J.-J. Hsu, I.J. Lowe, Spin–lattice relaxation and a fast T_1-map acquisition method in MRI with transient-state magnetization, J. Magn. Reson. 169 (2004) 270–278.
[4] H.Y. Carr, E.M. Purcell, Effects of diffusion on free precession in nuclear magnetic resonance experiments, Phys. Rev. 94 (1954) 630–638.
[5] D.P. Madio, I.J. Lowe, Ultra-fast imaging using low flip angles and FIDs, Magn. Reson. Med. 34 (1995) 525–529.
[6] D.P. Madio, H.M. Gach, I.J. Lowe, Ultra-fast velocity imaging in stenotically produced turbulent jets using RUFIS, Magn. Reson. Med. 39 (1998) 574–580.
[7] H.M. Gach, I.J. Lowe, Characterization of flow emerging from a stenosis using MRI, Magn. Reson. Med. 40 (1998) 559–570.
[8] J.-J. Hsu, I.J. Lowe, Signal recovery in free induction decay imaging using a stimulated spin echo, Magn. Reson. Med. 47 (2002) 409–414.
[9] G.H. Glover, S. Lai, Self-navigated spiral fMRI: interleaved versus single-shot, Magn. Reson. Med. 39 (1998) 361–368.
[10] D.C. Look, D.R. Locker, Time saving in measurement of NMR and EPR relaxation times, Rev. Sci. Instrum. 41 (1970) 250–251.
[11] H. Zhao, W.M. Westler, J.L. Markley, Precise determination of T_1 relaxation values by a method in which pairs of nonequilibrium magnetizations are measured across a constant relaxation period, J. Magn. Reson. A 112 (1995) 139–143.
[12] P.R. Bevington, D.K. Robinson, Data reduction and error analysis for the physical sciences, second ed., McGraw-Hill, Boston, Massachusetts, 1992.
[13] R.K. Breger, A.A. Rimm, M.E. Fischer, R.A. Papke, V.M. Haughton, T1 and T2 measurements on a 1.5-T commercial MR imager, Radiology 171 (1989) 273–276.
[14] K.P. Whittall, A.L. MacKay, D.A. Graeb, R.A. Nugent, D.K.B. Li, D.W. Paty, In vivo measurement of T_2 distributions and water contents in normal human brain, Magn. Reson. Med. 37 (1997) 34–43.
[15] P. Schmitt, M.A. Griswold, P.M. Jakob, M. Kotas, V. Gulani, M. Flentje, A. Haase, Inversion recovery TrueFISP: quantification of T_1, T_2, and spin density, Magn. Reson. Med. 51 (2004) 661–667.
[16] S.C.L. Deoni, T.M. Peters, B.K. Rutt, High-resolution T_1 and T_2 mapping of the brain in a clinically acceptable time with DESPOT1 and DESPOT2, Magn. Reson. Med. 53 (2005) 237–241.
[17] General Electric Company, Signa EXCITE HD operator manual, Revision 2 (English), Milwaukee, Wisconsin, 2005.

[18] R.K. Gupta, J.A. Ferretti, E.D. Becker, G.H. Weiss, A modified fast inversion–recovery technique for spin–lattice relaxation measurements, J. Magn. Reson. 38 (1980) 447–452.
[19] J.L. Evelhoch, J.J.H. Ackerman, NMR T_1 measurements in inhomogeneous B_1 with surface coils, J. Magn. Reson. 53 (1983) 52–64.
[20] I. Kay, R.M. Henkelman, Practical implementation and optimization of one-shot T_1 imaging, Magn. Reson. Med. 22 (1991) 414–424.
[21] J.-J. Hsu, G.H. Glover, Rapid time-series mapping of the longitudinal relaxation time of the brain during neuronal activity, in: Proc. Intl. Soc. Magn. Reson. Med., vol. 14, International Society for Magnetic Resonance in Medicine, 2006, p. 661.
[22] L.D. Diesbourg, F.S. Prato, G. Wisenberg, D.J. Drost, T.P. Marshall, S.E. Carroll, B. O'Neill, Quantification of myocardial blood flow and extracellular volumes using a bolus injection of Gd-DTPA: kinetic modeling in canine ischemic disease, Magn. Reson. Med. 23 (1992) 239–253.
[23] A.J. Freeman, P.A. Gowland, P. Mansfield, Optimization of the ultrafast Look–Locker echo-planar imaging T_1 mapping sequence, Magn. Reson. Imaging 16 (1998) 765–772.
[24] C.A. McKenzie, F.S. Prato, R.E. Thornhill, D.J. Drost, T_1 fast acquisition relaxation mapping (T_1-FARM): optimized data acquisition, Magn. Reson. Imaging 18 (2000) 129–138.
[25] P. Gowland, P. Mansfield, Accurate measurement of T_1 in vivo in less than 3 seconds using echo-planar imaging, Magn. Reson. Med. 30 (1993) 351–354.
[26] C.Y. Tong, F.S. Prato, A novel fast T1-mapping method, J. Magn. Reson. Imaging 4 (1994) 701–708.
[27] Z. Chen, F.S. Prato, C. McKenzie, T_1 fast acquisition relaxation mapping (T_1-FARM): an optimized reconstruction, IEEE Trans. Med. Imaging 17 (1998) 155–160.
[28] N.J. Shah, M. Zaitsev, S. Steinhoff, K. Zilles, A new method for fast multislice T_1 mapping, Neuroimage 14 (2001) 1175–1185.
[29] M.A. van Walderveen, R.A. van Schijndel, P.J. Pouwels, C.H. Polman, F. Barkhof, Multislice T_1 relaxation time measurements in the brain using IR-EPI: reproducibility, normal values, and histogram analysis in patients with multiple sclerosis, J. Magn. Reson. Imaging 18 (2003) 656–664.
[30] Y. Ishimori, H. Kimura, H. Uematsu, T. Matsuda, H. Itoh, Dynamic T1 estimation of brain tumors using double-echo dynamic MR imaging, J. Magn. Reson. Imaging 18 (2003) 113–120.
[31] M. Peller, V. Kurze, R. Loeffler, S. Pahernik, M. Dellian, A.E. Goetz, R. Issels, M. Reiser, Hyperthermia induces T_1 relaxation and blood flow changes in tumors: a MRI thermometry study in vivo, Magn. Reson. Imaging 21 (2003) 545–551.
[32] N.J. Shah, H. Neeb, M. Zaitsev, S. Steinhoff, G. Kircheis, K. Amunts, D. Häussinger, K. Zilles, Quantitative T_1 mapping of hepatic encephalopathy using magnetic resonance imaging, Hepatology 38 (2003) 1219–1226.
[33] R.G. Steen, M. Hunte, E. Traipe, P. Hurh, S. Wu, L. Bilaniuk, J. Haselgrove, Brain T_1 in young children with sickle cell disease: evidence of early abnormalities in brain development, Magn. Reson. Imaging 22 (2004) 299–306.
[34] A. Castriota-Scanderbeg, F. Fasano, M. Filippi, C. Caltagirone, T_1 relaxation maps allow differentiation between pathologic tissue subsets in relapsing–remitting and secondary progressive multiple sclerosis, Mult. Scler. 10 (2004) 556–561.
[35] S. Cho, D. Jones, W.E. Reddick, R.J. Ogg, R.G. Steen, Establishing norms for age-related changes in proton T_1 of human brain tissue in vivo, Magn. Reson. Imaging 15 (1997) 1133–1143.